

# Gas temperature measurements in weakly ionized glow discharges with filtered Rayleigh scattering

Azer P. Yalin, Yury Z. Ionikh, and Richard B. Miles

We report the first gas temperature measurements in plasmas to our knowledge obtained by filtered Rayleigh scattering (FRS). A narrow-linewidth Ti:sapphire laser is used as the illumination source, and a mercury filter provides strong suppression of elastic background. We perform measurements in weakly ionized glow discharges in pure argon and in an argon-plus-1%-nitrogen mixture. Where possible, we verify the FRS technique by comparing filtered measurements with unfiltered measurements. We present point measurements of axial temperature with uncertainties of less than 5%. We use a planar scheme to obtain radial temperature profiles with uncertainties of 10%. © 2002 Optical Society of America

OCIS Codes: 350.5400, 350.2450, 120.6780, 290.5870, 300.0300.

## 1. Introduction

In this paper we focus on measuring the gas temperature in low-pressure ( $\sim 50$ -Torr), weakly ionized glow discharges. The temperature fields in such discharges are of interest from the viewpoint of both basic plasma research,<sup>1</sup> and because of their connection to several specific engineering problems. One such problem is the interpretation of experimental results concerning shock wave propagation in diffuse plasmas (e.g., Refs. 2–4). Accurate knowledge of the gas temperature has enabled us to properly model the thermal effects and interpret the experimental results.<sup>5</sup>

A variety of nonintrusive optical diagnostics was used to perform neutral gas temperature measurements in plasmas. Interferometry and absorption techniques have found widespread use, but both are path-integrated measurements and therefore their application tends to be limited to axisymmetric cases. Furthermore, interferometric methods may need

phase-shift corrections and may have poor spatial resolution depending on the source used. Measurements by plasma emission are often possible, but also may be of limited spatial resolution. Laser-induced fluorescence offers excellent resolution; however, the challenge is to obtain accurate quantitative results. Effects of quenching and line-shape integrals often complicate quantitative analysis. A variety of nonlinear methods, such as coherent anti-Stokes Raman scattering (e.g., Refs. 6 and 7), laser-induced thermal anemometry,<sup>8</sup> and thermal grating methods,<sup>9</sup> can be used to perform point measurements, but they are inherently not well suited for two-dimensional imaging.

An alternative is to use a nonresonant scattering process, such as Rayleigh or Raman scattering. Rayleigh scattering, which is the elastic scattering of light by molecules, also has the potential for diagnostic measurements with excellent spatial resolution. However, because it is an elastic process, it is often difficult to separate any stray elastic background (that is due to windows, particulates, electrodes) from the scattering signal. The utility of Rayleigh scattering is greatly enhanced by use of a resonant atomic (or molecular) vapor filter, the technique then being termed filtered Rayleigh scattering (FRS). The scattered light is imaged through the vapor filter, and the signal measured at the detector is the spectral overlap of the scattered light with the filter transmission profile. The filter can serve two purposes. It strongly suppresses any stray elastic background and it gives a means of spectrally probing the scattering lineshape. The FRS technique has been success-

---

At the time of this research, A. P. Yalin (azer@saha.stanford.edu) and R. B. Miles were with the Department of Mechanical and Aerospace Engineering, Princeton University, Princeton, New Jersey 08544. A. P. Yalin is now with the Department of Mechanical Engineering, Stanford University, Stanford, California 94305-3032. Y. Z. Ionikh is with the Institute of Physics, St. Petersburg State University, St Petersburg, 198904, Russia.

Received 13 August 2001; revised manuscript received 11 January 2002.

0003-6935/02/183753-10\$15.00/0

© 2002 Optical Society of America

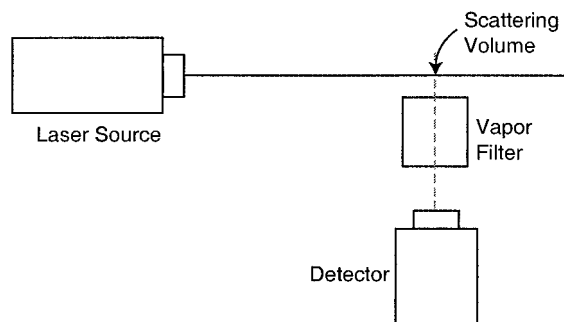


Fig. 1. Schematic diagram of the FRS setup. A narrow-linewidth laser is used to illuminate a sample volume, and the scattered light is imaged through a narrow-band atomic or molecular vapor absorption filter onto a detector.

fully used to perform planar measurement of temperature, density, and velocity to accuracies of several percent.<sup>10</sup> The technique has been demonstrated in numerous environments, for example, for temperature measurement in combustion (e.g., Refs. 11 and 12) and for velocimetry and flow visualization in high-speed flows.<sup>10</sup> For velocity measurements, a related technique, termed planar Doppler velocimetry, measures Doppler shifts with broadened vapor filters (e.g., Refs. 13 and 14). In this paper we apply the ultraviolet FRS technique toward the measurement of gas temperature in weakly ionized glow discharges. We previously verified the UV FRS technique for air temperature measurements,<sup>15</sup> and we now apply it to measurements in weakly ionized plasmas. To our knowledge, this is the first use of FRS in plasma environments. We study two weakly ionized diffuse discharges: a pure argon discharge as well as an argon plus 1% nitrogen discharge. When possible, we compare Rayleigh measurements with FRS measurements and find excellent agreement. Using a point measurement system, we perform FRS measurements of axial temperature as a function of current for the two mixtures. We also present the results of planar FRS measurements of radial temperature profiles. A discussion of the applicability and limitations of the technique is presented.

## 2. Filtered Rayleigh-Scattering Measurement Technique

The basic setup for FRS measurements is shown in Fig. 1. A narrow-linewidth laser is used to illuminate a sample volume, and the scattered light is imaged through a narrow-band atomic or molecular vapor absorption filter onto a detector. Point measurements can be obtained with a single-element detector, or the beam can be focused into a sheet and a multielement detector can be used to obtain planar measurements. The amount of scattered light incident on a detector element depends on the spectral overlap of the scattered light with the filter transmission profile. Essentially, the filter contains an atomic or molecular vapor and is strongly absorptive around the vapor resonances whereas it is transpar-

ent elsewhere. The scattered light consists of an elastic background component (typically from window scattering or stray reflections), as well as the Rayleigh light scattered from the plasma. In the absence of a filter, it is generally difficult (or impossible) to separate the Rayleigh-scattering signal from the elastic background. On the other hand, an appropriately chosen vapor filter provides a means of strongly suppressing any elastic background, so that virtually all the light reaching the detector is Rayleigh light. The width of the absorption feature is controlled so that it is wide compared with the laser linewidth (elastic scatter), yet comparable to the width of the Rayleigh-scattering lineshape. In this way, with the laser tuned to the middle of the absorption, the elastic light is strongly suppressed whereas a reasonably high (~40%) fraction of the Rayleigh light is transmitted. Suppression of any nonelastic background (which is due to, for example, pump lasers or sample luminosity) can be performed with conventional thin-film interference filters or monochromators.

Rayleigh-based measurement techniques are attractive for several reasons. Rayleigh scattering is a nonresonant process and thus unaffected by quenching and saturation. Furthermore, it is linear with scatterer density.<sup>16</sup> What remains is to relate the FRS signal to the plasma's gas temperature, and this is done through knowledge of the Rayleigh-scattering lineshape, which is the spectral profile of the scattering intensity. Generally, the Rayleigh-scattering lineshape has a temperature and pressure dependence. The exact nature of the profile is given by the dimensionless  $Y$  parameter, which reflects the relative contributions of uncorrelated and correlated molecular motions to the lineshape.<sup>10,17</sup> In the limit  $Y \ll 1$  (Knudsen regime), uncorrelated molecular motion dominates, and the resulting lineshape is Gaussian and independent of pressure. In the limit  $Y \gg 1$  (hydrodynamic regime), correlated molecular motion dominates, and acoustic features (sidebands) contribute to the lineshape. For the plasmas of current interest one finds  $Y \sim 0.01$ , meaning that the scattering lineshape is nearly Gaussian; however, in our analysis we do model the full lineshape. As mentioned above, the FRS signal is the overlap of the scattering lineshape (and background) with the filter transmission profile. Because the filter profile is well characterized, a model can be used to recover the gas temperature from the FRS signal. Along with background suppression, the vapor filter provides a means of probing the scattering lineshape.

We present a brief comparison between our research in the UV using a Ti:sapphire laser and a mercury filter at 254 nm with the more conventional research in the visible portion of the spectrum that uses a frequency-doubled Nd:YAG laser and an iodine filter at 532 nm. More detail can be found in Ref. 18. Operating in the UV allows us to capitalize on the higher Rayleigh-scattering cross section and the higher background suppression of the mercury filter. The scattering cross section scales nearly as

frequency to the fourth power. However, one must also consider the linear dependence of photon energy on frequency, so that the number of scattered photons for a given beam energy scales nearly as frequency to the third power. There is also a weak dependence on the depolarization factor. Combining these factors yields 10.7 times more Rayleigh-scattered photons at 254 nm than at 532 nm for a given beam energy. Standard photomultiplier tubes (PMTs) have comparable quantum efficiencies at the two wavelengths (approximately 25%) yielding an increase in counts of a factor of approximately 10 for a given beam energy. In practice, one can use a lower energy source in the UV than in the visible and still obtain as large or larger signal levels. Another important element in the comparison of filters is their background suppression. For a typical 5-cm mercury filter, the absorption of elastically scattered (resonant) light is modeled to be much greater than  $10^{10}$ , whereas for a typical 5-cm iodine filter the absorption is limited to approximately  $10^5$ .<sup>10</sup> The background suppression is particularly important in experiments where the background scattering is strong compared to the Rayleigh signal, such as when windows or walls are in close proximity to the sample volume or when many particulates are present. In such cases the stronger suppression makes the mercury filter far more attractive than iodine. The actual suppression achieved in the current study is discussed in Section 3.

### 3. Experiment

#### A. Approach and Signal Modeling

Depending on the given environment, the measurement approach can be slightly varied. Here, the approach is to ratio the FRS signal with the plasma on (at the temperature to be measured,  $T_M$ ) to the FRS signal at the same pressure but with the plasma off (at a reference temperature,  $T_{REF}$ ). We term this ratio as  $\mathcal{R}$ . The ratio approach allows us to normalize away most calibration factors (solid angle, quantum efficiency, window losses). Both measurements are taken at the same laser frequency, which is tuned to lie within an absorption notch of the filter so that the elastic background is continuously suppressed. At constant pressure there is a one-to-one correspondence of temperature and density, so assuming that we know the reference temperature  $T_{REF}$ , the measured FRS signal ratio uniquely defines the unknown temperature  $T_M$ . The signal ratio is primarily determined by the density ratio, with a smaller opposing contribution from lineshape effects. We present results of signal modeling for such an approach.

Figure 2 shows the modeled filter transmission profile and the modeled FRS signal levels as functions of laser frequency detuning for an argon plasma. The mercury vapor filter has a length of 5 cm, a mercury vapor pressure of 0.0030 Torr, and a temperature of 315 K. The various notches in the filter profile are due to hyperfine splitting and different isotopic contributions. The nominal location of

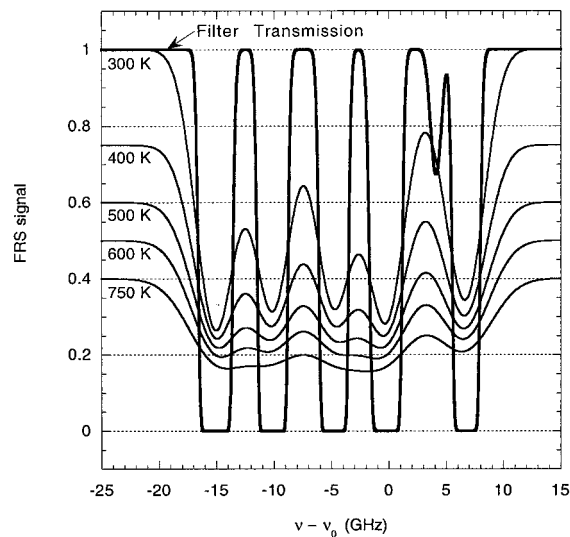


Fig. 2. Modeled FRS signal levels and filter transmission profile in the 253.7-nm vicinity. The mercury vapor filter has a length of 5 cm, a vapor pressure of 0.0030 Torr, and a temperature of 315 K. The modeled FRS signal levels are for a scattering gas of 50-Torr argon at the indicated temperatures.

the lines is at 253.7 nm. The filter transmission profile is found from Beer's law—more details (including experimentally measured filter transmission profiles) can be found in Refs. 18 and 19. The modeled FRS signal levels are for a scattering gas of 50-Torr argon at various temperatures and assume the simple 90-deg scattering geometry shown in Fig. 1. We use the S6 model developed by Tenti *et al.*<sup>17</sup> to compute the Rayleigh-scattering lineshape. The FRS signals are found as the convolution of the Rayleigh-scattering lineshape with the filter transmission profile; for more details and measured FRS signal profiles, see Refs. 10, 15, and 18. Profiles (scans) are not presented here, because in the current study we perform measurements by maintaining the laser frequency at the middle of the filter's absorption notch rather than scanning across it. The Rayleigh-scattering cross section is not affected by the weak ionization, so the FRS curves are valid for both gaseous and weakly ionized argon. The FRS signals are normalized relative to 300 K and 50 Torr. In the filter transmission, the FRS signals scale with the argon density (inverse temperature). However, when the laser is tuned to lie within an absorption feature, there is an additional signal-dependence effect that is due to the variation of scattering linewidth with temperature. In this case the signal is nearly, but not exactly, proportional to the scattering density. Figure 3 is a closer view of the highest-frequency absorption notch, which is used in the current experiments. The modeled FRS signal levels are shown, along with the laser frequency (indicated with an arrow) used in the current experiments. When we examine the FRS curves at different temperatures, it is straightforward to relate the unknown plasma temperature  $T_M$  to the experimentally

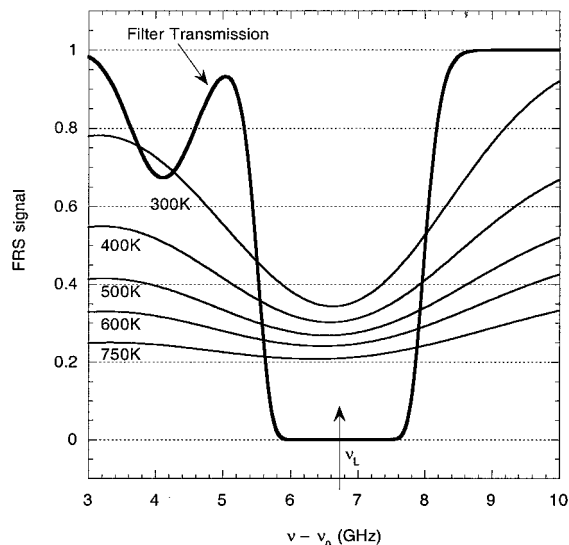


Fig. 3. Modeled FRS signal levels and filter transmission profile shown for the experimentally used (high-frequency) absorption notch. Parameters are as in Fig. 2. The arrow indicates the laser tuning used in the experiments.

measured ratio  $\mathcal{R}$ . Figure 4 is such a curve, plotted for the 50-Torr argon plasma, with the same mercury filter conditions as above, and plotted for a plasma-off temperature  $T_{REF} = 308$  K. The unknown temperature  $T_M$  corresponds to the plasma-on temperature. Also shown is the analogous curve for unfiltered Rayleigh scattering.

#### B. Plasma Source

A small-scale plasma facility has been developed in our laboratory. A 20-kV dc power supply is used to

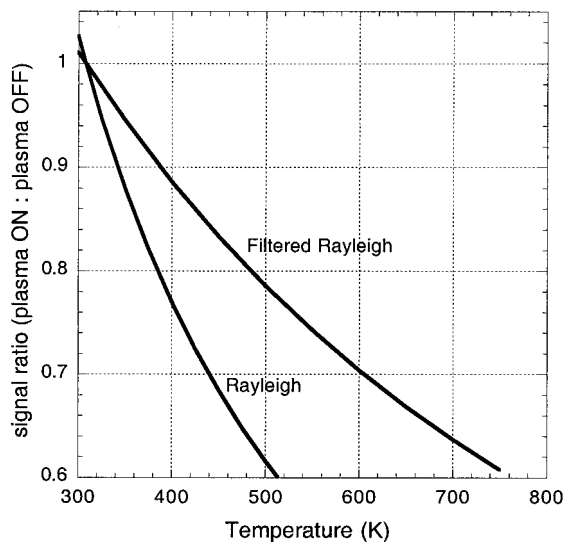


Fig. 4. Graph showing the curve to convert the FRS signal ratio  $\mathcal{R}$  (measured as plasma on:plasma off) to the unknown plasma-on temperature  $T_M$ , plotted for  $T_{REF} = 308$  K and for a scatterer of argon at 50 Torr. Also shown is the equivalent curve for unfiltered Rayleigh scattering.

sustain glow discharges in a discharge tube of diameter 38 mm (1.5 in.). The discharge tube is made of quartz, with antireflection coated windows. The coatings reduce the elastic scatter considerably. The electrode separation can be changed among 20, 40, and 60 cm, and the different separations can be used to measure the electric field in the plasma. Two measurements at different lengths are required so that the voltage drop at the electrodes can be subtracted. A flow-regulating system allows control of the gas mixture and flow rate. A type K thermocouple is used to measure the plasma wall temperature, and a Baratron pressure gauge (accuracy better than 1%) measures the cell pressure. Two one-dimensional translation stages can be used to translate the discharge tube horizontally relative to the laser beam.

We perform measurements in two types of discharge: pure argon and an argon plus 1% nitrogen mixture. The discharges are selected to replicate the conditions used in plasma shock wave propagation experiments (e.g., Refs. 3 and 4). We operate at conditions in which the discharges are diffuse or volumetric (not contracted or filamentary). At 50-Torr pressure, this limited the current in the argon discharge to a maximum of approximately 35 mA, whereas the mixture did not contract at currents as high as 200 mA. Our experimental results show that the current distribution in the plasmas echoes this behavior.

#### C. Filtered Rayleigh-Scattering Configuration

The experimental configuration is illustrated in Figs. 5(a) and 5(b). A high-power, tunable, narrow-linewidth Ti:sapphire laser<sup>19</sup> is used as the excitation source. The frequency-tripled output is delivered to the plasma tube through several antireflection-coated beam-shaping optics. For these experiments pulse energies of approximately 10 mJ in the UV (253.7 nm) were used. The beam passes through a half-wave plate to ensure the correct orientation of the linearly polarized beam and through a quarter-wave plate to correct for the slight elliptical polarization introduced at the tube windows. Several irises are used to reduce stray light carried with the beam.

For point measurements [Fig. 5(a)], a long focal-length lens (90 cm) is used to weakly focus the beam to a waist of approximately 200  $\mu\text{m}$  at the sample volume. The sample volume is within the discharge tube and is defined by the laser beam waist and an iris located between the discharge tube and the collection lens ( $f$ -number of 2.4). The sample volume has a length of approximately 1 mm. The scattered light is collected at 90 deg with the collection lens and passes through the mercury vapor filter. The filter is 5 cm long and has two temperature controllers yielding a vapor pressure of 0.0030 Torr and a filter temperature of 315 K (for more detail, see Ref. 19). At these conditions, the filter is modeled to have a suppression of resonant light of greater than  $10^{10}$ . However, in our experiments the actual background suppression is limited not by the filter, but by the

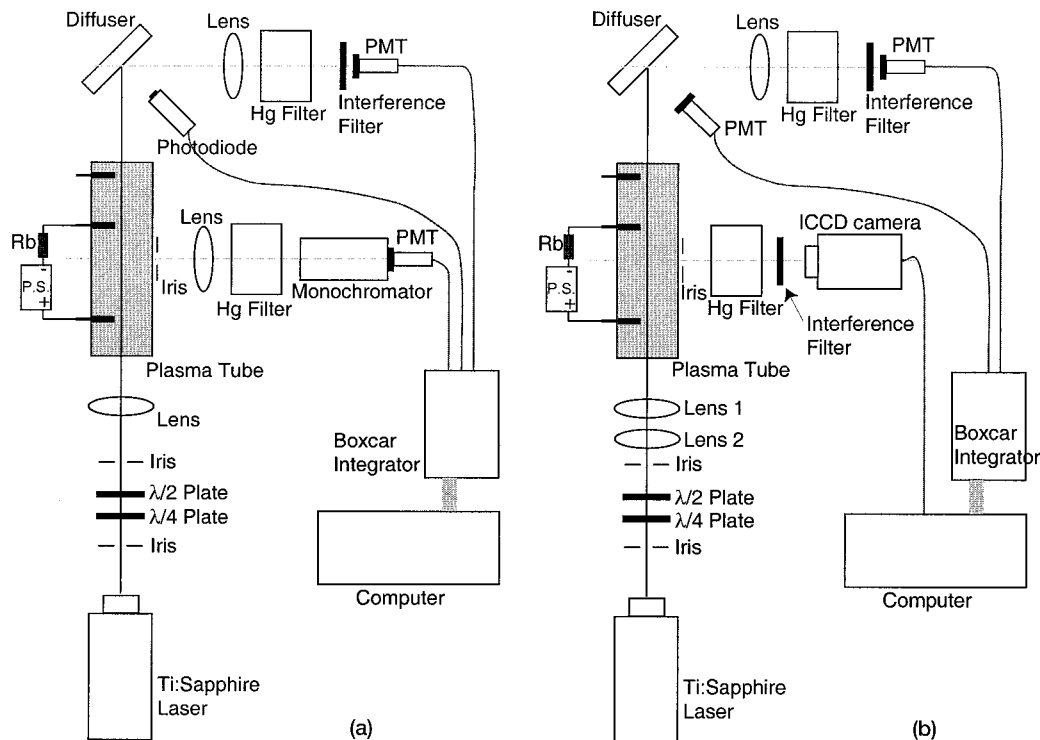


Fig. 5. Schematic diagram of experimental setups used for (a) point and (b) planar FRS measurements of plasmas. The experiments use the same laser and plasma tube; however, they differ in beam delivery optics and detection system. For the point measurements in (a) we use a monochromator to suppress plasma luminosity and a PMT as the detector. The planar scheme in (b) uses an interference filter to suppress plasma luminosity and a gated intensified CCD (ICCD) camera as the detector.

spectral purity of the laser source: Any broadband (impure) component of light within the laser pulse (that is spectrally broad compared to the filter's absorption notch) is not absorbed. Clearly, a spectrally pure laser source is desirable. Using related methods, we measured the spectral purity (seeding efficiency) of our laser source to be approximately 0.998 (or approximately 499 parts in 500).<sup>20</sup> By imaging elastically scattered laser light through the filter and scanning the laser wavelength, we can measure the overall experimental suppression of our system also as 500 to 1. In other words, with the laser tuned to the filter absorption, we are unable to detect any transmission of light through the filter except for that which we expect because of the impurity of the laser source. Thus we conclude that the filter suppression is large compared with 500 to 1, as expected. (To measure the actual filter suppression, a laser source with higher spectral purity is required.) We find that, with the plasma tube evacuated (and the laser tuned to the middle of the absorption notch), there is no measured signal. Thus the system suppression is sufficiently strong that the elastic scatter background signal is negligible. After the mercury filter, the light passes through a monochromator, which acts as a broad-passband filter, while rejecting plasma luminosity and other colors of light from the laser. Finally, the scattered light signal is collected with a Hamamatsu R960 PMT. The plasma luminosity signal, after passing through the monochromator,

was negligibly small. A picked-off beam illuminates a diffuser and is measured through a second mercury filter (frequency reference), as well as by a photodiode (power reference). The latter two measurements use thin-film interference filters (Corion G25-254-F) for spectral filtering. The three signals are collected with a boxcar onto a computer. We verified the system linearity by performing measurements at varying gas pressure (with the plasma off). At pressures in the range of 20–100 Torr, the linearity was better than 2–3%. The uncertainty of measurements is discussed further in Section 4.

The planar measurements use a modified scheme, shown in Fig. 5(b). Essentially, the difference is that the laser is focused into a sheet instead of a line, and the PMT is replaced with an intensified CCD camera. Each pixel, or resolution element, of the camera corresponds to its own sample volume in the plasma and can be independently analyzed by the methods described above. A short focal-length (7.5-cm) positive cylindrical lens is arranged confocally with a long focal-length (90-cm) positive spherical lens to form the laser into a sheet of width roughly 2 cm and a waist of approximately 200  $\mu\text{m}$ . The scattered light is imaged through the mercury vapor filter. Because a two-dimensional image is being captured, we replace the monochromator slit with a thin-film interference filter (Corion G50-254-F). The interference filter acts as a broad-passband filter, while rejecting the plasma luminosity and pump la-

ser light. The intensified CCD camera is a Princeton Instruments Pentemax system. It is gated to a width of 50 ns, and the pixels are binned to form resulting pixels corresponding to  $0.9 \text{ mm} \times 0.9 \text{ mm}$  in the discharge. A reference leg is set up similar to that used in the point measurements. In the planar experiment, the backgrounds (laser scatter and discharge emission) are no longer negligible, so that the data acquisition and analysis has some added complexity relative to the point case. The laser background is higher because the laser energy is distributed across numerous sample volumes, so that higher detector gain is used, and the laser sheet and discharge tube geometry generates significantly more elastic scatter. It is important that this laser scatter background is due to the parasitic broadband (unseeded) component within the laser pulse (which is not suppressed by the filter). We can make this determination by looking at the dependence of the background light on the laser frequency and by knowing the spectral purity of the laser source. Improving the spectral purity of our laser source (e.g., Refs. 21 and 22) would alleviate this problem. Also, we have an appreciable plasma background in the planar measurements because we use an interference filter rather than a monochromator to attenuate the plasma luminosity. These backgrounds are measured and appropriately subtracted in the data processing. The uncertainty of measurements is discussed further in Section 4.

#### 4. Results and Discussion

##### A. Comparison of Filtered Rayleigh-Scattering and Rayleigh Data

Plasma temperature as a function of discharge current was measured along the axis of an argon and argon plus 1% nitrogen plasma. The plasmas were both at a pressure of 50 Torr. Initially, we picked one discharge condition, argon at 50 Torr and 20 mA, and performed point measurements of the axial temperature using both FRS and conventional (unfiltered) Rayleigh scattering. These measurements provided further verification of the accuracy of the FRS technique. For example, Fig. 6 shows a series of Rayleigh and FRS measurements of the axial temperature in the argon plasma. We performed the FRS measurements by ratioing the signal levels with the plasma on and off, as discussed above. The elastic background was strongly suppressed by the filter, and no background subtraction was required. On the other hand, the Rayleigh measurements suffered from elastic background, and therefore a background subtraction step was required. We measured the background by collecting the signal with the discharge tube at vacuum. Note that, in cases in which the elastic background is high—for example, if the laser beam is near to the cell wall or electrodes—measurements without the filter become inaccurate or impossible. The mean and standard deviations of both sets of measurements are shown. The mean of the Rayleigh and FRS values differ by 1% (less than

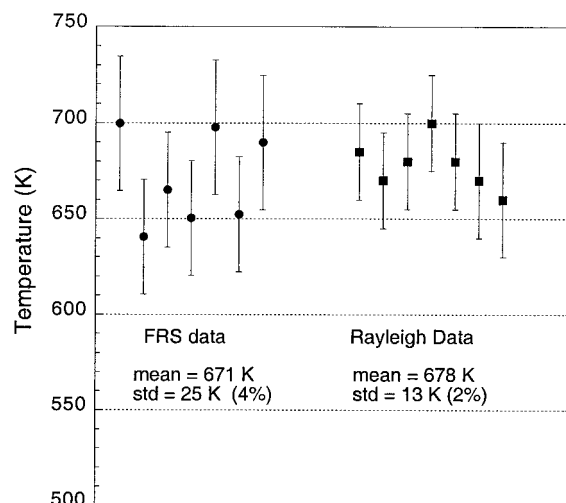


Fig. 6. Comparison of FRS measurements (circles) and Rayleigh measurements (squares) of axial temperature of argon discharge. The discharge conditions were at a pressure of 50 Torr and a current of 20 mA. Computed means and standard deviations (std) of the data are given.

experimental uncertainty). The standard deviation of the FRS measurements is 4% and is slightly higher than for the unfiltered data because of drift in the laser frequency, as well as the slightly declined sensitivity. Additional verification of the agreement between the filtered and the unfiltered measurements can be seen in Figs. 7 and 8.

##### B. Variation of Plasma Axial Temperature with Current

Axial temperatures were measured as a function of current for both the argon and the argon and nitrogen mixture. The results, along with computed curves,

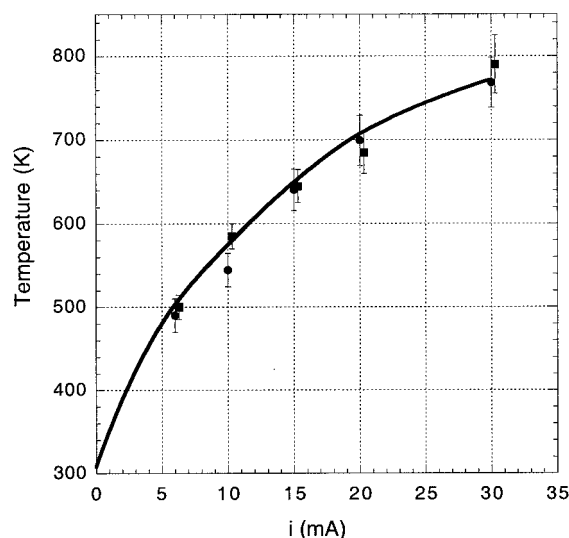


Fig. 7. FRS measurements (circles) of axial temperature in a 50-Torr argon discharge at a range of currents. Rayleigh-scattering data (squares) are also shown. The curve is a calculated temperature profile assuming a Gaussian current-density profile.

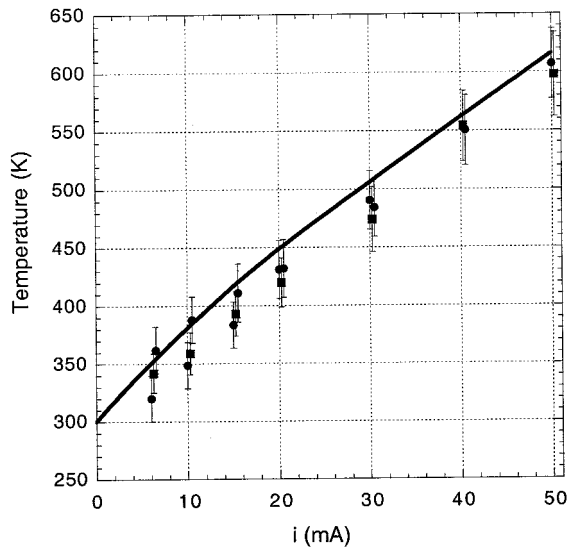


Fig. 8. FRS measurements (circles) of axial temperature in a 50-Torr argon plus 1% nitrogen discharge at a range of currents. Rayleigh-scattering data (squares) are also shown. The curve is a calculated temperature profile assuming a Bessel current-density profile.

are shown in Figs. 7 and 8. Figure 7 shows axial temperature measurements for different values of current for the pure argon plasma. The plasma temperatures range from approximately 480 K at 6 mA up to approximately 770 K at 30 mA. Data shown are both by FRS (circles) and Rayleigh (squares) methods. Figure 8 shows axial temperature measurements at different values of current for an argon plus 1% nitrogen mixture. Again, data shown are both by FRS (circles) and Rayleigh (squares) methods. For the mixture, the temperatures are lower than for the pure argon and range from approximately 340 K at 6 mA to approximately 600 K at 50 mA.

Measuring the wall temperature, as well as the current and voltage ( $E$  field) of the discharges, allows us to perform gas temperature calculations. We calculate the gas temperature profile by solving the thermoconductivity equation for an infinite-length cylinder:

$$\frac{1}{r} \frac{d}{dr} \left[ r \eta(T) \frac{dT}{dr} \right] + \beta j(r) E = 0, \quad (1)$$

with the usual boundary conditions  $T(r)|_R = T_w$  and  $dT/dr|_0 = 0$ . Here,  $R$  is the discharge tube radius,  $T_w$  is the wall temperature,  $E$  is the electric field,  $j(r)$  is the current density,  $\eta$  is the thermal conductivity of argon, and  $\beta$  is the fractional energy transfer from electrons to the translational motion of atoms, i.e., to gas heating. For both argon and argon with 1% nitrogen admixture, and for the temperature range 300–1100 K,  $\eta(T)$  can be approximated by the linear function  $[8.8 + 0.0348 \times T(\text{K})] \times 10^{-3} \text{ W m}^{-1} \text{ K}^{-1}$ .<sup>23</sup> For glow discharge plasmas in rare gases at intermediate pressures,  $\beta$  is known to be close to 1.<sup>1</sup> For

molecular gases, and mixtures of molecular gases with rare gases, typically  $\beta < 1$ .<sup>24</sup> This is true, however, for high concentrations of the molecular component (tens of percent). In our case of small molecular addition (1%) we do not expect a significant influence on the  $\beta$  value and we adopt  $\beta_{\text{Ar+N}_2} = \beta_{\text{Ar}} = 1$ .

The current-density profile is determined differently for pure argon and the argon plus nitrogen mixture. In the latter case the discharge looks quite uniform, and therefore the usual Bessel form is adopted:

$$j(r) = j_0 J_0(2.405 r/R), \quad (2)$$

where  $j_0$  is  $j$  at  $r = 0$  and  $J_0$  is the zeroth-order Bessel function. (The Bessel profile actually describes the electron number density rather than current density, but the slight difference between them is neglected here.) The experimentally measured current is used to normalize (scale) the profile. The calculated curve in Fig. 8 is found accordingly from Eq. (1) and is in good agreement with the experimental data. The half-width at half-maximum of the profile is  $0.63R$ . The discharge in pure argon appears essentially less uniform, with a marked decrease in luminosity intensity from the center to the wall. Attempts to apply a Bessel profile to  $j(r)$  result in a large discrepancy with the experimental results, both in axial values and radial dependences. For the pure argon discharge we use a Gaussian function (truncated to zero at the wall):

$$j(r) = j_0 \frac{\exp\left[-\left(\frac{r}{a}\right)^2\right] - \exp\left[-\left(\frac{R}{a}\right)^2\right]}{1 - \exp\left[-\left(\frac{R}{a}\right)^2\right]}, \quad (3)$$

with a fitting parameter  $a$ . For  $a = 1$  it gives a profile with a half-width of  $0.62R$ , which is close to the profile of Eq. (2). Smaller values of  $a$  correspond to narrower profiles. We find that, at a pressure of 50 Torr, the Gaussian profile of Eq. (3) with  $a = 0.43 \pm 0.03$  yields the best fit to the experimental temperature data (both the axial temperatures and the radial profiles). The half-width of such a profile is  $(0.36 \pm 0.03)R$ . We calculated the computed temperature profile shown in Fig. 7 from Eq. (1) assuming this current-density profile.

To have a physical basis for the Gaussian current distribution, we compare the calculated rates per unit length for ionization  $I$  and electron losses  $L$  in the positive column of an argon glow discharge at a pressure of 50 Torr and a current below that required for transition to a contracted discharge. A kinetic model for the argon discharge plasma at moderate pressures was developed by a number of authors (see, e.g., Refs. 25–27). At these conditions, ionization is primarily due to electron collisions with metastable argon atoms, which in turn are formed by electron excitation and destroyed in three-body collisions with argon atoms. The main electron loss mechanism is a dissociative recombination with  $\text{Ar}_2^+$  ions, the lat-

ter being the dominant ion at these conditions. The electron energy distribution function was calculated for our conditions by Dyatko *et al.* (see details in Ref. 28). Cross sections and rate constants for all the mentioned processes are found in Refs. 27 and 29. Our simulation shows that satisfactory agreement between  $I$  and  $L$  is achieved for values of the  $\alpha$  parameter between 0.39 and 0.48 ( $I$  and  $L$  differ by less than a factor of 2). For  $\alpha = 0.43$  the difference between the computed ionization and the loss rates is less than 30%. These results show that the adopted current distribution is quite reasonable.

The differing forms of the current profiles in the argon and argon and nitrogen discharges are likely due to different ionization mechanisms in the two plasmas. In the latter case excited nitrogen molecules are likely involved. The differing ionization mechanisms also lead to the weaker electric field strength in the argon and nitrogen discharge, which is the reason for the lower gas temperature in this case as compared with the argon plasma at the same current. The current distribution found in the argon plasma is narrower than that of the mixture (0.36  $R$  versus 0.63  $R$ ). This is consistent with the pure argon plasma being at conditions much closer to contraction. Recall that at 50 Torr the argon discharge contracts at approximately 35 mA whereas the mixture remains diffuse at 200 mA. We performed similar measurements for other admixtures of nitrogen,<sup>18</sup> and found that there is a certain admixture (order 1% nitrogen) that yields a minimum temperature, which is less than that in either pure argon or pure nitrogen.

### C. Radial Profile of Plasma Temperature

Diffuse discharges were studied in argon and in an argon plus 1% nitrogen mixture, both at a pressure of 50 Torr. The argon discharge was measured at a current of 20 mA. The resulting temperature field from one measurement (256 shots) is shown in Fig. 9(a). The vertical direction in Fig. 9(a) is aligned with the plasma axis, whereas the horizontal direction corresponds to the radial axis of the plasma. The field of view in the radial direction is slightly asymmetric with respect to the plasma axis, whereas the field of view in the axial direction is approximately in the center of the discharge, between the two electrodes. The temperature range is approximately 680 K on axis to approximately 600 K at the right of the image. The apparent temperature variation in the axial direction is assumed to be an artifact of the measurement (laser sheet variations) and not due to actual variations in plasma temperature in that direction. The measurement uncertainty ( $\sim 10\%$ ) is comparable to the relative temperature gradient in the measurement region ( $\sim 12\%$ ), making it difficult to see the shape of the temperature field. The plasma was mounted horizontally in the laboratory; however, we did not observe any effects of buoyancy. The data points in Fig. 10(a) show the result of the temperature field averaged from several images along the axial direction. A radial extent (or step size) of 0.9 mm was used for each averaged point, whereas

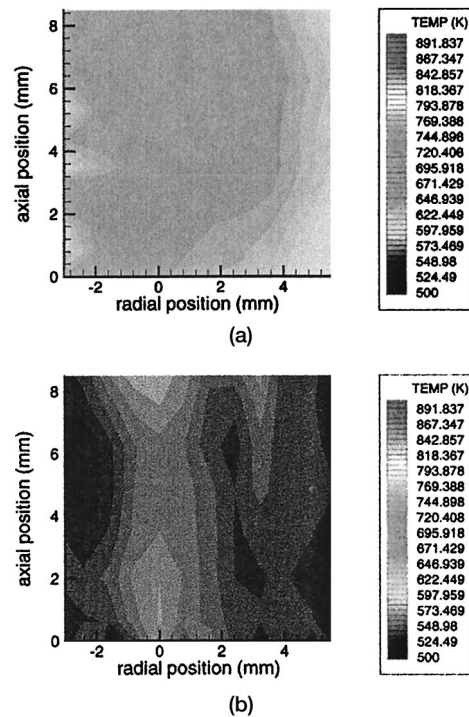


Fig. 9. (a) Temperature image of a diffuse argon plasma obtained by planar FRS. The tube radius is 19 mm, the pressure is 50 Torr, and the current is 20 mA. (b) Planar FRS temperature image of a diffuse argon plus 1% nitrogen plasma at the same conditions except with a current of 40 mA.

all data in the axial direction were included. Vertical error bars are due to the deviation in the data, whereas the horizontal error bars are due to the imprecision in the position of the sheet. Also shown is a curve that is a fit to temperature profiles that we obtained from point measurements. We obtained point measurements of radial temperature by displacing the discharge tube relative to the optical axis.) The planar method has the significant advantage that the whole profile can be obtained in a single measurement. The planar data are in good agreement with the point results. We find the data to be fit well with the Gaussian current distribution described above.

Several researchers have studied similar argon glow discharges. In Ref. 30, Golubovskii *et al.* measured temperature profiles with an interferometric method, which required various corrections. For example, heating of the windows generates some phase shift and was measured separately. For a similar argon discharge, they measured an axial temperature of 570 K, but calculated a temperature of 700 K. Our axial temperature of 680 K is reasonably consistent with their model.

As we saw in Subsection 4.B, the addition of a small amount of nitrogen to the argon causes a decrease in temperature and an increase in the width of the current distribution. Figure 9(b) shows a temperature image obtained from the argon plus 1% nitrogen mixture. Again, the vertical direction is aligned with the plasma axis, whereas the horizontal direction corre-

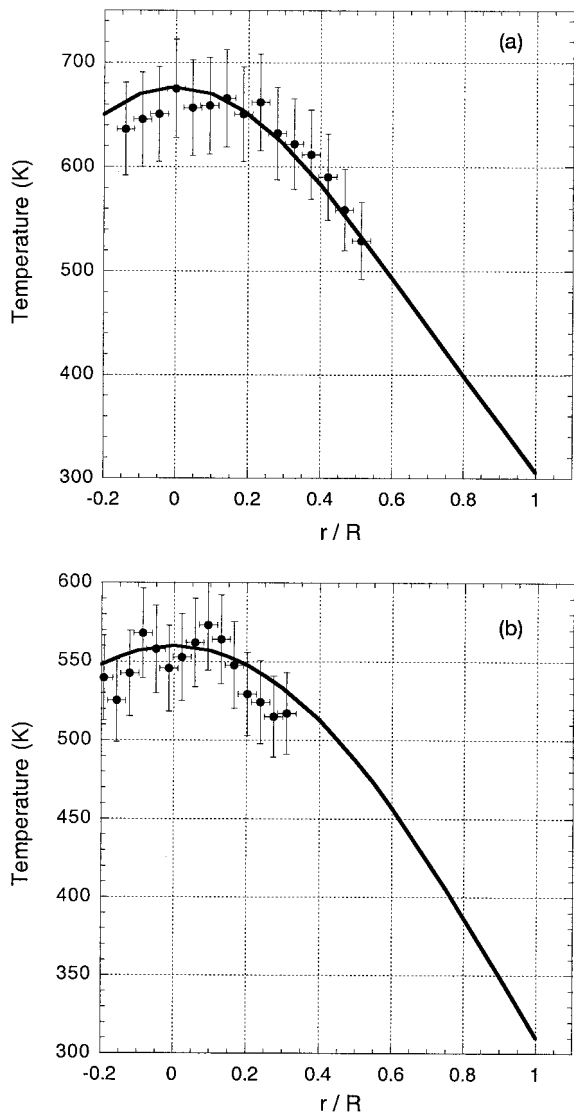


Fig. 10. (a) Radial temperature profile of the diffuse argon plasma obtained by planar FRS. Conditions are as in Figs. 9(a) and 9(b). The data points are found when we average across the image of Fig. 9(a), whereas the curve shown is a fit to the point measurements. (b) FRS temperature profile of the diffuse argon plus 1% nitrogen plasma. The points are found when we average across the image of Fig. 9(b), whereas the curve is a fit to the point measurements.

sponds to the radial axis of the plasma. The field of view in the radial direction is slightly asymmetric with respect to the plasma axis, whereas the field of view in the axial direction is approximately in the center of the discharge, between the two electrodes. The axial temperature is approximately 550 K. Figure 10(b) shows the results of the temperature averaged along the axial extent, at constant radial positions, from several images. Also shown is a solid curve, found as a fit to the results of point measurements. The radially averaged planar values are in good agreement with point measurements. We find the data to fit well with the Bessel current distribution described above. As discussed, the difference in temperature and current distributions between the argon and the argon and

nitrogen mixture is likely connected to the difference in electric field strength and ionization mechanisms.

#### D. Uncertainty Analysis

We considered the uncertainties in the point measurements. We found that the point temperature measurements had standard deviations of approximately 4%, which was primarily due to drift in the seed laser. The uncertainty in the determination of the FRS signal ratio was approximately 2–3%, however, combining this with the temperature dependence resulted in a temperature uncertainty of approximately 4%. The magnitude of the FRS signal level depends on the precise tuning (order of 10–100 MHz) of the laser source relative to the absorption filter, and in these experiments the seed laser was not externally locked. The spatial resolution was approximately 0.5 mm and was due to imprecision in the position of the laser beam relative to the discharge tube.

The planar measurements had uncertainties of approximately 10%. We performed statistics on the image files to understand the origin of this uncertainty. The signal ratio  $\mathcal{R}$  is typically found to an accuracy of approximately 7%, which yields a 10% error in temperature (because of the slope of the conversion curve). We found that there are three primary, and nearly equal, sources of this uncertainty: the signal measured with the plasma on, the signal measured with the plasma off, and the laser scatter background signal measured at vacuum. The uncertainty in the first two cases is primarily due to drift of the seed laser, as well as shot-to-shot fluctuations in the laser sheet profile (because of a damaged third-harmonic crystal), whereas the uncertainty in the third case stems largely from noise in the seeding process. Improving the seed laser drift, laser sheet profile, and reducing the laser background (by reducing the scatter or improving the laser spectral purity), we should be able to reduce the measurement uncertainty. The background that is due to plasma luminosity has a negligible contribution to the overall measurement uncertainty.

#### E. Applicability of Technique

We consider the range of applicability of the FRS technique in terms of plasma conditions. We have demonstrated temperature measurements in weakly ionized discharges at temperatures in the range of 300–700 K. To some extent the filter can be tailored to the temperature range of interest. We find that reasonable sensitivity (greater than 50% of the ideal theoretical value) can be obtained at temperatures up to approximately 1000 K. At higher temperatures the presence of adjacent isotopic features leads to a gradual drop in sensitivity. Our measurement system has a detection limit of the order of 1 Torr. Measurements at elevated pressures should not pose any difficulty, whereas measurements below approximately 1–10 Torr will have increased noise. Finally, we consider the effect of the ionization fraction. The current approach requires that the Rayleigh-

scattering cross section be the same for the gas as it is for the plasma. Rayleigh-scattering cross sections for ionized species are generally not well known so it is difficult to place an exact upper bound on the ionization fraction. However, typical glow discharges have ionization fractions less than one part in a million,<sup>1</sup> which should easily satisfy the requirement. One of the strengths of the technique (in contrast to path-integrated measurements) is that it can be used to probe plasmas with essentially no symmetry. Along with the diffuse glow discharge measurements, we have performed measurements in contracted (filamentary) glow discharges.<sup>18</sup>

## 5. Conclusion

We have demonstrated use of the FRS technique as an optical diagnostic to measure gas temperature in weakly ionized glow discharges. We examined two discharges, one in argon and another in an argon plus 1% nitrogen mixture. In cases with low elastic background we were able to compare FRS measurements with unfiltered measurements and found good agreement. We performed measurements of axial temperature versus current in the two discharges, as well as measurements of radial temperature profiles. Measurement uncertainties were approximately 4% for point measurements and 10% for planar measurements.

The authors acknowledge A. V. Meshchanov for his assistance, as well as the U.S. Air Force Office of Scientific Research for funding.

## References

1. Y. P. Raizer, *Gas Discharge Physics* (Springer, Berlin, 1987).
2. P. A. Voinovich, A. P. Ershov, S. E. Ponomareva, and V. M. Shibkov, "Propagation of weak shock waves in plasma of longitudinal flow discharge in air," *High Temp.* **29** (3), 468–475 (1991).
3. B. N. Ganguly, P. Bletzinger, and A. Garscadden, "Shock wave damping and dispersion in nonequilibrium low pressure argon plasmas," *Phys. Lett. A* **230**, 218–222 (1997).
4. A. R. White and V. V. Subramaniam, "Effect of wall shear on the propagation of a weak spark-generated shock wave in argon," *Phys. Fluids* **13**, 2441–2444 (2001).
5. Y. Z. Ionikh, N. V. Chernysheva, A. V. Meshchanov, A. P. Yalin, and R. B. Miles, "Direct evidence for thermal mechanism of plasma influence on shock wave propagation," *Phys. Lett. A* **259**, 387–392 (1999).
6. M. Bruchhausen, J. Voigt, T. Doerk, S. Hadrich, and J. Uhlenbusch, "Resonant coherent anti-Stokes Raman scattering applied to vapor phase InI," *J. Mol. Spectrosc.* **201** (1), 70–82 (2000).
7. T. M. Yoshida, T. M. Jovin, and B. G. Barisas, "Resonance coherent anti-Stokes Raman scattering in nitrogen-dioxide using a broadband dye-laser," *Opt. Eng.* **34**, 2631–2636 (1989).
8. E. B. Cummings, "Laser-induced thermal acoustics—simple accurate gas measurements," *Opt. Lett.* **19**, 1361–1363 (1994).
9. P. F. Barker, J. H. Grinstead, and R. B. Miles, "Single-pulse temperature measurement in supersonic air flow with predisassociated laser-induced thermal gratings," *Opt. Commun.* **168**, 177–182 (1999).
10. J. N. Forkey, "Development and demonstration of filtered Rayleigh scattering—a laser based flow diagnostic for planar

- measurements of velocity, temperature, and pressure," Ph.D. dissertation (Department of Mechanical Engineering and Aerospace, Princeton University, Princeton, N.J., (1996).
11. D. Hoffman, K. U. Munch, and A. Leipertz, "Two-dimensional temperature determination in sooting flames by filtered Rayleigh scattering," *Opt. Lett.* **21**, 525–527 (1996).
12. G. S. Elliot, N. Gluma, C. D. Carter, and A. S. Nejad, "Two-dimensional temperature field measurements using a molecular filter based technique," *Combust. Sci. Technol.* **125**, 351–357 (1997).
13. M. W. Smith, G. B. Northam, and J. P. Drummond, "Application of absorption filter planar Doppler velocimetry to sonic and supersonic jets," *AIAA J.* **34** (3), 434–441 (1996).
14. G. S. Elliot, M. Samimy, and S. A. Arnette, "A molecular based velocimetry technique for high speed flows," *Exp. Fluids* **18**, 107–118 (1994).
15. A. P. Yalin and R. B. Miles, "Temperature measurements by ultraviolet filtered Rayleigh scattering using a mercury filter," *J. Thermophys. Heat Transfer* **14** (2), 210–215 (1999).
16. A. C. Eckbreth, *Laser Diagnostics for Combustion Temperature and Species* (Abacus, Kent, UK, (1998).
17. G. Tenti, C. D. Boley, and R. C. Desai, "On the kinetic model description of Rayleigh-Brillouin scattering from molecular gases," *Can. J. Phys.* **54**, 285–297 (1972).
18. A. P. Yalin, "Gas phase and plasma diagnostics based on resonant atomic vapor filters," Ph.D. dissertation (Department of Mechanical Engineering and Aerospace, Princeton University, Princeton, N.J., 2000).
19. N. D. Finkelstein, "An ultraviolet laser source and spectral imaging filters for non-intrusive laser based diagnostics," Ph.D. dissertation (Department of Mechanical Engineering and Aerospace, Princeton University, Princeton, N.J., 1998).
20. A. P. Yalin, P. F. Barker, and R. B. Miles, "Characterization of laser seeding by use of group-velocity dispersion in an atomic-vapor filter," *Opt. Lett.* **25**, 502–504 (2000).
21. C. K. Ni and A. H. Kung, "Effective suppression of amplified spontaneous emission by stimulated Brillouin scattering phase conjugation," *Opt. Lett.* **21**, 1673–1675 (1996).
22. L. P. Bakker, J. M. Freriks, F. J. de Hoog, and G. M. W. Kroesen, "Thomson scattering using an atomic notch filter," *Rev. Sci. Instrum.* **71**, 2007–2014 (2000).
23. J. Kestin, K. Knierim, and F. A. Mason, "Equilibrium and transport properties of the noble gases and their mixtures at low density," *J. Phys. Chem. Ref. Data* **13** (1), 229–303 (1984).
24. M. Capitelli, ed, *Nonequilibrium Vibrational Kinetics* (Springer-Verlag, Berlin, 1986).
25. B. Yu. Golubovskii and R. Sonnenburg, "The positive column in an argon discharge," *Sov. Phys. Tech. Phys.* **24** (2), 177–180 (1979).
26. G. M. Petrov and C. M. Ferreira, "Numerical modeling of the constriction of the dc positive column in rare gases," *Phys. Rev. E* **59**, 3571–3582 (1999).
27. A. A. Matveev and V. P. Silakov, "Electron energy distribution function in a moderately ionized argon plasma," *Plasma Sources Sci. Technol.* **10** (1), 134–146 (2001).
28. N. A. Dyatko, Yu. Z. Ionikh, N. B. Kolokolov, A. V. Meshchanov, and A. P. Napartovich, "Jumps and bi-stabilities in electron energy distribution in Ar-N<sub>2</sub> post discharge plasma," *J. Phys. D* **33**, 2010–2018 (2000).
29. E. V. Karaulova and Yu. A. Lebedev, "Computer simulation of microwave and DC plasmas: comparative characterization of plasmas," *J. Phys. D* **25** (3), 401–412 (1992).
30. Y. B. Golubovskii, Y. M. Kagan, and V. N. Rzhetskii, "Atomic temperature measurements in a positive discharge column for intermediate pressures in inert gases," *Opt. Spectrosc.* **41**(5) 221–223 (1976).